DEVELOPMENT OF 3D HEAT TRANSFER AND PYROLYSIS IN FDS

Randall McDermott[1,4], Chao Zhang[1], Morgan Bruns[2], and Salah Benkorichi[3]

[1]National Institute of Standards and Technology, Gaithersburg, Maryland, USA
[2]Virginia Military Institute, Lexington, Virginia, USA
[3]Omega Fire Engineering Ltd., Manchester, UK
[4]e-mail: randall.mcdermott@nist.gov

ABSTRACT

The condensed phase in FDS is presently modeled using a 1D heat conduction solver in-depth normal to the surface of the solid. The solid is given a thickness and the boundary condition on the "backing" of the solid is taken either from another surface, or, if the backing is "exposed" and if the solid is one cell thick, the thermal conditions from the FDS gas phase domain may be applied. The 1D approximation limits the accuracy of the surface boundary conditions when FDS is used for structural analysis. It also prevents pre-heating of the surface for lateral and downward flame spread. In this paper, we will discuss the implementation of a 3D heat transfer model in FDS. Pyrolysis kinetics have been added to the 3D conduction solver. Material properties use the same input formats as the 1D solver. Residue formation (e.g., char) and burn away are possible in the 3D pyrolysis model. An interior heat flux "wall model" for the 3D conduction solver allows for accurate estimation of the surface heat flux without prohibitively high grid resolution in the solid phase. The model is fully parallel and integrated with FDS outputs for slice files, boundary files, and devices.

INTRODUCTION

Historically, the Fire Dynamics Simulator (FDS) has been limited to one-dimensional (1D) heat transfer (conduction) internal to the solid or condensed phase. While this assumption is adequate for a broad class of problems, accurate thermal analysis of structural components in a fire, tracking flame fronts in smoldering combustion, and modeling lateral or downward flame spread all require solid phase heat transfer in multiple dimensions. In this paper, we describe the initial formulation, implementation, and verification of a 3D heat transfer and pyrolysis model in FDS, which is presently in *beta* testing.

The relevant prior work in this area includes two different 3D heat transfer implementations into alternate FDS branches as well as two other multi-dimensional pyrolysis models. In his 2009 thesis at RWTH Aachen University, Andreas Vischer published a 3D heat transfer model, which at the time was implemented in FDS 5 [1]. His code has since been integrated into FDS 6, but not merged with the master branch maintained by the FDS developers. A parallel effort to implement a 3D heat transfer module in FDS was undertaken by the Institute for Building Materials, Solid Construction and Fire Protection (iBMB) at Technische Universtät Braunwchweig [2]. The initial module was implemented for FDS 5 by Volker Hohm and revised for FDS 6 by Matthias Siemon. While there was some discussion
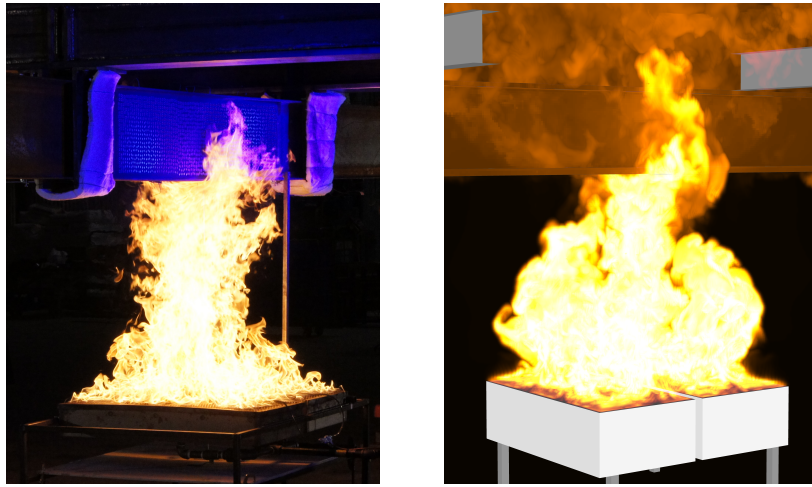
Figure 1: NIST large fire laboratory commissioning test. (Left) Large-scale experiment studying the interaction between a 700 kW fire and mechanically-loaded building elements. Photo by Lisa Choe. (Right) FDS volume rendering of heat release rate. Heat transfer in the I-beam is modeled with the new 3D solver including lateral heat conduction.

with the authors in 2016 about merging these heat transfer modules, unfortunately, this effort did not crystallize.

In terms of multi-dimensional pyrolysis models, Stanislav Stoliarov's group at the University of Maryland develops *Thermakin* [3], which can handle 2D solids. Chris Lautenberger of *Reax Engineering* develops and maintains *Gpyro* [4], which has 3D capabilities *and* can in principle be coupled with FDS 6.

We chose to implement our own model for several reasons. First, the project started as a simple proof-of-concept attempt to capture lateral heat transfer in the I-beam used in the NIST large fire research laboratory commissioning tests [5] (see Fig. 1). From the start, our new implementation of 3D heat transfer has been built to integrate with the current parallel computing capabilities in FDS. Also, the new model works seamlessly with FDS DEVC ("device"), BNDF ("boundary file"), and SLCF ("slice file") outputs.

Another reason to implement our own model is to have more control over the formulation and development. The more we have learned about the subtleties of modeling thermally degrading materials in 3D, the more we have realized that the numerical schemes needed for shrinking and swelling materials in multi-dimensions are not straight-forward, and the choices made in how to deal with intumescence and burn away can have leading-order effects on the model results.

The remainder of this paper is organized as follows. We first present the governing equations for heat transfer, mass transfer, and reaction kinetics used in the 3D model. This includes special consideration for continuous flux boundaries. Last, we present several verification cases.

MATHEMATICAL FORMULATION

This section describes the governing equations for heat and mass transfer in the new 3D solver. Mass transfer in the present context may be considered instantaneous, as in the current 1D model, or the user may choose to solve a diffusion equation. In-depth radiation may be treated using an optically

thick approximation [6], as discussed below.

Heat Transfer

Let k_s, ρ_s, and c_s denote, respectively, the thermal conductivity, density, and specific heat of the solid. The thermal properties may be functions of temperature. The mean temperature of an Eulerian cell in the solid phase is denoted T_s. The heat flux vector (may include radiation) is $\dot{\mathbf{q}}''$ and the volumetric heat source, either specified or from chemical reaction, is denoted $\dot{q}_s'''$. The governing equation for heat transfer is

$$\rho_s c_s \frac{\partial T_s}{\partial t} = -\nabla \cdot \dot{\mathbf{q}}'' + \dot{q}_s''' \tag{1}$$

Equation (1) is discretized with a second-order finite-volume scheme for fluxes and time integrated with explicit Euler, with an update taking place during the *corrector* step of the overall FDS time integration scheme (the temporal accuracy is therefore at best first-order). The temperature is stored in the cell center using the same array that houses the gas phase cell temperatures. The time step is chosen to be the minimum of the large-eddy simulation (LES) time step, δt, and the time step required for a Von Neumann number of VN = 0.5 in order to satisfy accuracy and stability constraints (see FDS Tech Guide [7]).

Heat Flux

The intercell fluxes are continuous. If the OBST material properties of neighboring cells are the same, then thermal properties at face centers are taken as linear averages when computing the intercell flux. The intercell flux at time level n may be obtained from either of the following (in practice the first relationship is used):

$$\dot{q}_{x,i+\frac{1}{2}}'' = -k_s \frac{\partial T_s}{\partial x}\bigg|_{i+\frac{1}{2}} \approx -k_{s,i} \frac{T_{s,i+\frac{1}{2}}^n - T_{s,i}^n}{\frac{1}{2}\delta x_i} = -k_{s,i+1} \frac{T_{s,i+1}^n - T_{s,i+\frac{1}{2}}^n}{\frac{1}{2}\delta x_{i+1}} \tag{2}$$

If the neighboring cells (this includes cells at mesh interfaces) have different material properties (consider the x direction with cell indices i and $i+1$), then the cell interface temperature, $T_{s,i+\frac{1}{2}}$, is computed using

$$T_{s,i+\frac{1}{2}}^n = \frac{T_{s,i}^n + \left[\frac{k_{s,i+1}}{k_{s,i}}\frac{\delta x_i}{\delta x_{i+1}}\right] T_{s,i+1}^n}{1 + \left[\frac{k_{s,i+1}}{k_{s,i}}\frac{\delta x_i}{\delta x_{i+1}}\right]} \tag{3}$$

which reduces to a simple linear average if $k_{s,i} = k_{s,i+1}$ and $\delta x_i = \delta x_{i+1}$.

Heat Flux with Local Material Deformation

As a material shrinks or swells, the distance between material points decreases or increases. It is challenging to handle this behavior on a static Eulerian grid. Consider the situation depicted in Fig. 2 where the material is shrinking. As the temperature points move closer, the effect is to increase the intercell heat flux. The flux becomes

$$\dot{q}_{x,i+\frac{1}{2}}'' \approx -k_{i+\frac{1}{2}} \frac{T_{s,i+1} - T_{s,i}}{\frac{1}{2}(\delta\tilde{x}_i + \delta\tilde{x}_{i+1})} \tag{4}$$

Calculation of the cell volumes, $\delta\tilde{x}$, etc., for pyrolysis with material deformation is discussed below.
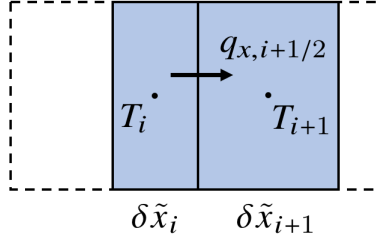
Figure 2: Diagram of intercell heat flux with a shrinking material.

Boundary Conditions

For two-way coupling between the gas and solid phase the boundary condition is continuity of heat flux and temperature. On the gas phase side, the heat fluxes are due to convection and radiation, and on the solid phase side the heat flux is due to conduction. The surface temperature links all these fluxes at an instant in time. Let T_w denote the interface temperature between the gas and solid, the face temperature of the "wall cell". The temperature at the cell center of the first solid cell is T_s. Let $\dot{q}''_{r,in}$, $\dot{q}''_{r,out}$, and $\dot{q}''_c$ denote the radiative flux to a surface, the radiative flux from a surface, and the convective heat flux, respectively. The flux continuity boundary condition then implies

$$\dot{q}''_{r,in} - \dot{q}''_{r,out} + \dot{q}''_c = -k_s \left. \frac{\partial T_s}{\partial n} \right|_w \tag{5}$$

To obtain the surface temperature, we take $\dot{q}''_{r,in}$ from the radiation solver, linearize $\dot{q}''_{r,out}$, and use Newton's law of cooling for $\dot{q}''_c$. The flux condition may then be discretized as

$$(\dot{q}''_{r,in})^n + 3\varepsilon^n \sigma (T_w^n)^4 - 4\varepsilon^n \sigma (T_w^n)^3 T_w^{n+1} + h^n(T_g^n - T_w^{n+1}) = -2 k_s^n \frac{T_s^n - T_w^{n+1}}{\delta} \tag{6}$$

where ε is the surface emissivity, σ is the Stefan-Boltzmann constant, δ is the linear thermal penetration depth (discussed below), h is the convective heat transfer coefficient, T_g is the gas temperature in the first off-wall grid cell and n indicates the time level in the simulation. Our result for the updated boundary temperature is

$$T_w^{n+1} = \frac{(\dot{q}''_{r,in})^n + 3\varepsilon^n \sigma (T_w^n)^4 + h^n T_g^n + 2 k_s^n T_s^n / \delta}{4\varepsilon^n \sigma (T_w^n)^3 + h^n + 2 k_s^n / \delta} \tag{7}$$

Surface Heat Flux Internal Wall Model

In Eqs. (6) and (7), the conductive heat flux into the wall is presumed to be resolved by a length scale, δ. In the 3D heat transfer model this length scale is *not* taken to be the 3D cell spacing normal to the wall—the required 3D grid resolution would make the model intractable. Instead, an internal wall model is employed. To be consistent with the resolution of the 1D heat conduction model, the thermal penetration depth is taken to be

$$\delta = \sqrt{\frac{\tau k_s}{\rho_s c_s}} \tag{8}$$

where τ is a somewhat arbitrary time scale set to unity.

Internal Radiation

The *absorption coefficient* of the solid is denoted κ_s. If $\delta \times \kappa_s \gg 1$, the material may be considered "optically thick" [6]. This applies to many problems in pyrolysis. The optically thick approximation implies a "radiative conductivity",

$$k_r = \frac{16 n_s^2 \sigma T_s^3}{3\kappa_s} , \tag{9}$$

which may simply be added to the material conductivity in the solver. Note that increasing the solid conductivity reduces the surface temperature, per Eq. (5), consistent with the notion that the radiation is not absorbed at the surface. Here, n_s is the material refractive index and σ is the Stefan-Boltzmann constant.

Pyrolysis

To begin our discussion of pyrolysis it is useful to start with definitions of the material mass density and volume. We consider a solid composed of a mixture of material components α. The *material density* (a property of the material) is

$$\rho_\alpha \equiv \frac{m_\alpha}{V_\alpha} \tag{10}$$

The *bulk density* is

$$\rho_{s,\alpha} \equiv \frac{m_\alpha}{V_s} \tag{11}$$

And the *total solid density* is

$$\rho_s \equiv \sum_\alpha \rho_{s,\alpha} \tag{12}$$

The bulk density of material component α evolves by

$$\frac{\partial}{\partial t}\left(\frac{\rho_{s,\alpha}}{\rho_s(0)} \right) = -\sum_{\beta=1}^{N_{r,\alpha}} r_{\alpha\beta} + S_\alpha \tag{13}$$

where $N_{r,\alpha}$ is the number of reactions consuming α. If α is a residue material, S_α represents the production rate. Note: the 3D pyrolysis code makes a call to the same kinetics subroutine as the 1D solver. So, there is nothing new to present here. The reaction rate $r_{\alpha\beta}$ (consumption of component α in reaction β) is discussed in detail in the FDS Tech Guide [7].

The heat source term due to chemical reactions (or phase change reactions) in the solid (or liquid) is given by

$$\dot{q}_s''' = -\rho_s(0) \sum_{\alpha=1}^{N_m} \sum_{\beta=1}^{N_{r,\alpha}} \Delta h_{\alpha\beta} r_{\alpha\beta} \tag{14}$$

where $\Delta h_{\alpha\beta}$ is the heat of reaction (heat of vaporization).

Local Material Deformation

A discussion about how the 1D model handles shrinking and swelling materials can be found in the FDS Tech Guide [7]. In this section, we deal with the same issue in 3D. One of the key differences in the 1D and 3D models is that the concept of "thickness" in the 1D model is not dependent at all on the 3D

computational mesh. In the 1D solver, the material shrinks from the bottom up, with the face of the solid stationary (until the cell potentially burns away).

Conversely, in 3D the solid mass is tied to the Eulerian grid cell. The grid cell itself cannot disappear. Instead we track the solid volume relative to the local cell volume. This volume ratio may be computed from the material densities as follows:

$$\phi_s \equiv \frac{V_s}{V_{cell}} = \frac{\Sigma_\alpha V_\alpha}{V_{cell}} = \sum_\alpha \frac{m_\alpha/\rho_\alpha}{m_\alpha/\rho_{s,\alpha}} = \sum_\alpha \frac{\rho_{s,\alpha}}{\rho_\alpha} \tag{15}$$

We presently consider two simple models for material deformation: isotropic and unidirectional. The method is based on the definition $V_s = \phi_s V_{cell}$, which is equivalent to $\prod_i \delta \tilde{x}_i = \phi_s \prod_i \delta x_i$. For a 2D case, if the material deforms equally in both directions (isotropic) then the spacing used to compute heat fluxes is computed from

$$\delta \tilde{x} = \phi_s^{1/2} \delta x$$
$$\delta \tilde{y} = \phi_s^{1/2} \delta y \tag{16}$$

If, on the other hand, we have a preferred direction for mass loss (such as in a cone calorimeter test), then the deformation is considered unidirectional. The flux spacing is computed as (deformation in x)

$$\delta \tilde{x} = \phi_s \delta x$$
$$\delta \tilde{y} = \delta y \tag{17}$$

Mass Transport

The movement of pyrolysis gas through the material to the solid surface is complicated to model in detail. In many practical codes, such as FDS, mass transfer resistance is simply ignored. Thus, any gas generated via pyrolysis is imagined to instantaneously appear at the solid surface as a mass flux boundary condition to the gas phase. The 3D model allows both instantaneous transport and diffusive transport, which we discuss below.

Gas Generation

The mass generation rate per unit volume of pyrolysis gas component γ in cell i, j, k is given by

$$\dot{m}'''_{\gamma,i,j,k} = \rho_s(0)_{i,j,k} \sum_{\alpha=1}^{N_m} \sum_{\beta=1}^{N_{r,\alpha}} \nu_{\gamma,\alpha\beta} r_{\alpha\beta,i,j,k} \tag{18}$$

Instantaneous Transport

Similar to the 1D model, instantaneous transport is the default mode of operation in the 3D model. However, implementation is not as straight-forward in 3D since Eulerian cells more than one cell below the surface are not usually tied to a "wall cell". In 3D, unless the user specifies otherwise, mass is ejected via the nearest wall cell and the deformation model is taken to be isotropic. Alternatively, the user may specify the direction for mass ejection and the deformation model becomes unidirectional.

For instantaneous transport, the mass flux at the solid surface for a given wall cell is the summation of the mass production in the column of solid cells tied to the wall cell. For a column of cells in the z direction tied to wall cell w, we have

$$\dot{m}''_{\gamma,w} = \sum_{k \in w} \dot{m}'''_{\gamma,i,j,k}\, \delta z_k \tag{19}$$

Diffusive Transport

A less arbitrary way to assign the pyrolysis gas to a wall cell is to simply solve a transport equation. While the physics is not so simple in reality, an isotropic diffusion model of transport has several advantages: It is easy to implement. It avoids any ad hoc assumptions applied in the instantaneous model. It handles smoldering combustion and char oxidation naturally. And finally, while the physics are not perfect, they are usually qualitatively correct and the implementation lends itself to improvement.

The diffusive transport equation for gas component γ is given by

$$\frac{\partial \rho_\gamma}{\partial t} = -\nabla \cdot \mathbf{J}_\gamma + \dot{m}'''_\gamma \tag{20}$$

where the diffusive flux is modeled with Fick's law,

$$\mathbf{J}_\gamma = -D_\gamma \tilde{\nabla} \rho_\gamma \tag{21}$$

Note that the gradient operator is written in terms of a deformed space coordinate, in the same manner as the heat flux. In the current implementation, the diffusivity is isotropic. The default is the gas phase molecular value for component γ. However, the user may adjust this value if needed.

Transport Boundary Conditions

Consider the flux between solid cell i and gas phase cell $i + 1$. The surface is denoted by F for "face value". The mass flux at the solid surface is taken from

$$J_{\gamma,\mathrm{F}} = -D_{\gamma,\mathrm{F}} \frac{\rho_{\gamma,\mathrm{F}} - \rho_{\gamma,i}}{\frac{1}{2}\delta \tilde{x}_i} \tag{22}$$

where

$$\rho_{\gamma,\mathrm{F}} = \begin{cases} 0 & \text{if } \gamma \text{ is fuel} \\ \rho Y_{\gamma,\mathrm{F}} & \text{if } \gamma \text{ is oxidizer} \\ \rho_{\gamma,i} & \text{if boundary is impermeable, } J_{\gamma,\mathrm{F}} = 0 \end{cases} \tag{23}$$

The boundary conditions in Eq. (23) provide qualitatively correct behavior for the pyrolysis gases (transport *out* of the solid) while allowing diffusion of oxidizer into the solid. Using $\rho Y_{\gamma,\mathrm{F}}$ for the fuel can lead to erratic behavior caused by diffusion of fuel back into the solid, which is not physical. This ad hoc treatment of the boundary is a limitation of the diffusion model, but we note that the scheme is no worse than the instantaneous transport out of the solid used in most 1D models.

It should be noted that $\rho Y_{\gamma,\mathrm{F}}$ is currently taken from the gas phase solver at the current time level. The mass flux is therefore time lagged between the gas phase and solid phase solvers, unlike the surface temperature from Eq. (7). This is a potential source of error that will be addressed in future development.

VERIFICATION TESTS

Heat Transfer

Continuous Heat Flux Boundary

In this test case, we utilize the non-steady state conduction solution provided in Carslaw and Jaeger [8] for a semi-infinite slab exposed to a constant ambient temperature, T_∞, with a constant convective heat transfer coefficient, h, and no radiation (see also Drysdale [9], Eq. (2.25)). The initial temperature of the slab, T_0, is set to 1000 °C. The thermal properties of the slab, $k = 1$ W/(m · K), $\rho = 1000$ kg/m^3, and $c = 0.001$ kJ/(kg · K), are set to give a thermal diffusivity, α, of 0.001 m^2/s. The analytical solution for this problem for the solid temperature, $T(x, t)$, is given by

$$\frac{T - T_0}{T_\infty - T_0} = \text{erfc}\left(\frac{x}{2\sqrt{\alpha t}}\right) - \exp\left(\frac{xh}{k} + \frac{\alpha t}{(k/h)^2}\right) \text{erfc}\left(\frac{x}{2\sqrt{\alpha t}} + \frac{\sqrt{\alpha t}}{k/h}\right) \tag{24}$$

where $\text{erfc} = 1 - \text{erf}(x)$.

This is a 1D problem in-depth into the solid. In FDS, the problem is solved in 2D, with the temperature varying in the x coordinate direction; there is no variation in the vertical, z, direction. While the solution is provided for a semi-infinite slab, FDS must use a finite thickness. The slab is taken to be 0.5 m in-depth, with $x = 0$ m marking the interface location between the fluid and the solid. The analytical solution for $T(x = 0.5, t)$ is used as the "back" boundary condition of the slab. The grid resolution is chosen to be 5 cm (10 cells covering 0.5 m). The stability constraint for the time step in the heat equation is therefore, $\delta t \leq \delta x^2/(2\alpha) = 1.25$ s. This is set as the initial time step in FDS, since no gas phase solution is computed.

Figure 3 shows the surface (wall) temperature, T_w, plotted as a function of time (the hot slab is cooling). Note that the exact solution for the surface temperature is taken from Eq. (24) with $x = 0$ m. That is, $T_w(t) \equiv T(0, t)$.
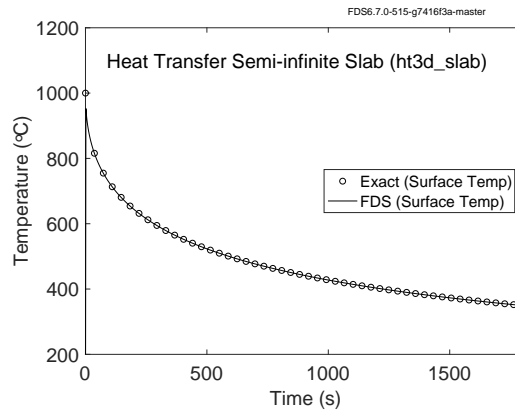

Figure 3: Test of continuous heat flux boundary condition for 3D heat transfer.

8

Heat Diffusion in a Steel I-Beam

The purpose of this test case is to compare FDS HT3D with a well-established commercial finite-element model (FEM) (ANSYS[1]) for a reasonably practical problem. We consider a steel I-beam cross-section 0.4 m on each side. The flanges are 6 cm thick and the web is 4 cm thick. The grid resolution for both FEM and FDS models is $\Delta x = 1$ cm. The FEM elements are hexagonal. The thermal properties of the steel are taken to be constant: $k = 45$ W/(m · K), $\rho = 7850$ kg/m^3, and $c = 0.60$ kJ/(kg · K). The boundary conditions are adiabatic except for a hot patch on the front half of the bottom flange maintained at 800 °C. The initial temperature of the steel is 20 °C and the case is run for 3600 s. Note that the FEM model is run with a time step comparable to the explicit stability criterion ($\Delta t \approx 1.7$ s) in order to yield time accurate results for comparison with FDS.

Figure 4 shows a comparison between the surface temperature contours from ANSYS (left) and FDS (right). Below that, in Fig. 5, we show the time history of the surface temperatures for six locations on the bottom flange (positions may be identified from the image on the left).
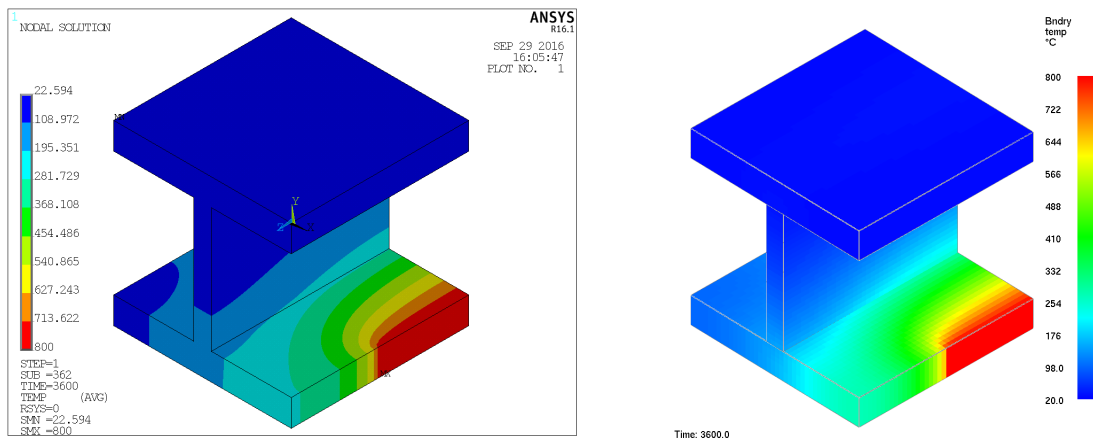

Figure 4: Three-dimensional heat diffusion in an I-beam, comparison between a commercial finite-element code (ANSYS, left) and FDS (right). The beam boundary conditions are adiabatic except for a hot patch maintained at 800 °C on the front right of the bottom flange.

Heat Diffusion in a Sphere

In this example, a solid sphere of radius 0.1 m with internal heat generated at $\dot{q}''' = 200$ kW/m^3 is studied. The initial temperature at the boundary is set to 20 °C. The objective of the test is to ensure that the heat conduction through the sphere and across the radius is computed properly. The heat conduction can be written as

$$\frac{\partial T}{\partial t} = \alpha \left[\frac{1}{r^2} \frac{\partial}{\partial r^2} \left(r^2 \frac{\partial T}{\partial r} \right) + \frac{\dot{q}'''}{k} \right] \tag{25}$$

---

[1]Any mention of commercial products within this paper is for information only; it does not imply recommendation or endorsement by NIST.
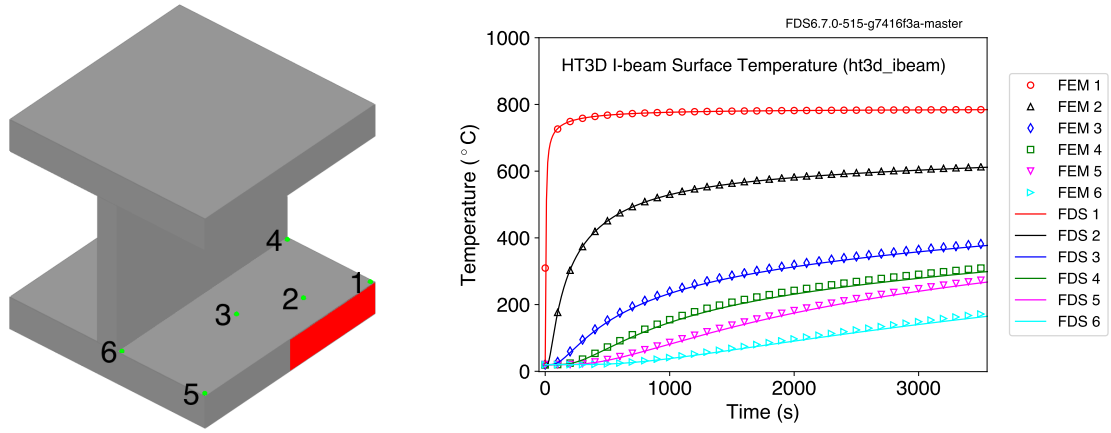
Figure 5: (Left) Device locations corresponding to the legend entries in the plot to the right. (Right) Time history of the surface temperature. Symbols represent the finite-element model (FEM) results and the lines represent the FDS results.

where k is the thermal conductivity and α is the thermal diffusivity. The initial and boundary conditions are

$$T|_{t=0} = T_0 \qquad ; \qquad T|_{r=a} = T_0 \qquad ; \qquad \left.\frac{\partial T}{\partial r}\right|_{r=0} = 0 \tag{26}$$

where T_0 is the initial temperature and a is the radius of the sphere. The exact solution to Eqs. (25) and (26) is from [8] (Sec. 9.8, p. 243):

$$T = T_0 + \frac{\dot{q}'''}{6k}\left(a^2 - r^2\right) + 2\frac{\dot{q}'''a^3}{k\pi^3 r}\sum_{n=1}^{\infty}\frac{(-1)^n}{n^3}\sin\left(\frac{n\pi r}{a}\right)\exp\left(-\alpha t\frac{n^2\pi^2}{a^2}\right) \tag{27}$$

The solution is run for 180 s. In Fig. 6 we show the temperature contours at $t = 165$ s for the medium resolution case (left) and a comparison between the analytical and numerical solutions at several points in time for the high resolution case (right).
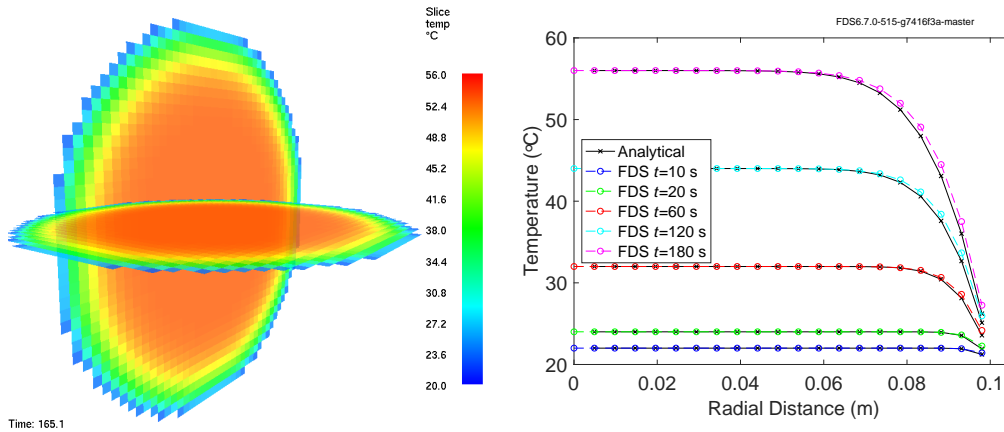

Figure 6: (Left) Temperature contours at $t = 165\,s$ for $n = 51$ cells across diameter. (Right) A comparison between radial profiles of the analytical and numerical solution at various times in the simulation.

10

Pyrolysis

Char Formation

This case is a simple mass conservation test for pyrolysis of wood into char and gas. A small block of wood, 0.08 m on a side, is heated externally at 50 kW/m^2 on all sides. Gas phase combustion is suppressed. The pyrolysis stoichiometry splits the wood to equal parts by mass of char and gas. In Fig. 7, one can see that the pine wood mass goes to zero, the char ends up with half the original wood mass, and the pyrolyzate gas production is equal to the char production.
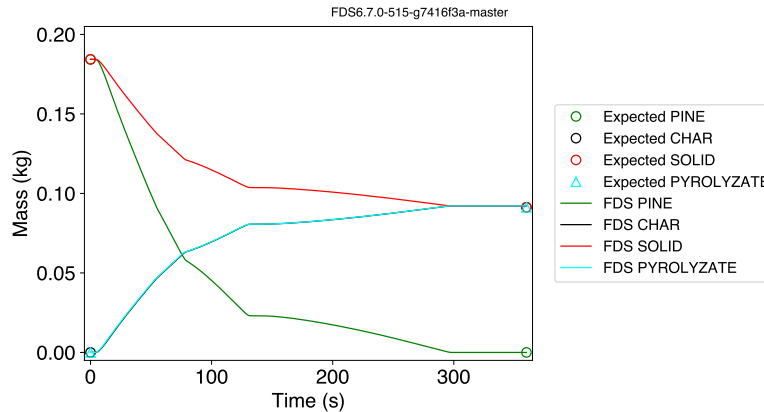

Figure 7: Conversion of wood to char and pyrolyzate gas with 3D solid heat transfer and pyrolysis.

Burn Away

This case is a replicate of the `box_burn_away1` case used as verification of the 1D pyrolysis solver. A foam block 0.4 m on a side (0.064 m^3) with a bulk density of 20 kg/m^3 (total mass of 1.28 kg) is heated from a wall kept at 1000 °C. The gas phase (and hence 3D solid phase) grid resolution is relatively coarse, $\delta x = 0.1$ m. However, the cell spacing for the 1D solver is internally computed to be approximately 3×10^{-3} m. The 1D solver thus resolves the temperature gradient near the surface on the inside of the solid. The 3D solver uses an internal wall model to enhance the heat flux into the solid cell. The verification target here is simply the total mass of 1.28 kg. Results are shown for the 3D solver with and without mass transport of fuel gas. In the latter, the gas is ejected to the nearest wall cell upon pyrolysis.

Mass Loss Rate and Thickness

This case compares mass loss rates and material thickness for pyrolysis of black PMMA between the 1D pyrolysis solver without burn away and the 3D solver with burn away. The 3D solver is effectively solving a 1D problem, so the results should be very similar. In-depth radiation absorption is not considered. The problem is set up with insulating sides for each column of material. The material is heated from the top with an external flux of 50 kW/m^2. The material thickness is 0.01 m. The grid resolution of the 3D solver is set to be equivalent to the node spacing for the 1D solver, $\delta z = 2.8571 \times 10^{-4}$ m. The key difference between the solvers is that in the 1D solver the top face of the `OBST` does not move, instead the material thickness changes and shrinks from the bottom up. Conversely, in the 3D solver, cells burn away as their mass goes to zero. If the material mass of a given cell goes below a threshold,
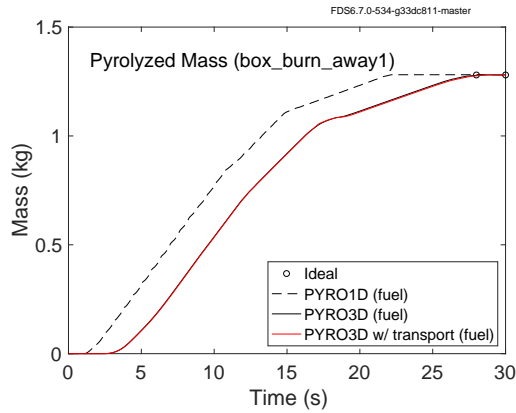
Figure 8: Comparison of burn away for 1D and 3D pyrolysis solvers. Verification target is total mass. Rate of pyrolysis varies between the methods due to the surface heat flux boundary condition and the difference in grid resolution.

the mass is shifted to a neighboring cell before the cell is burned away. The final cell burns down to a numerical threshold mass before that mass is finally clipped for numerical reasons. We still track the local solid volume within a cell, and this ratio times the cell size gives a measure of the material thickness for the 3D solver. Fig. 9 shows mass loss rate per unit area (left) and the material thickness (right) for the 1D and 3D solutions. Note that in the 3D solution the "thickness" is taken as the integral of the volume ratio $V_{\text{solid}}/V_{\text{cell}}$ over the height of the column.
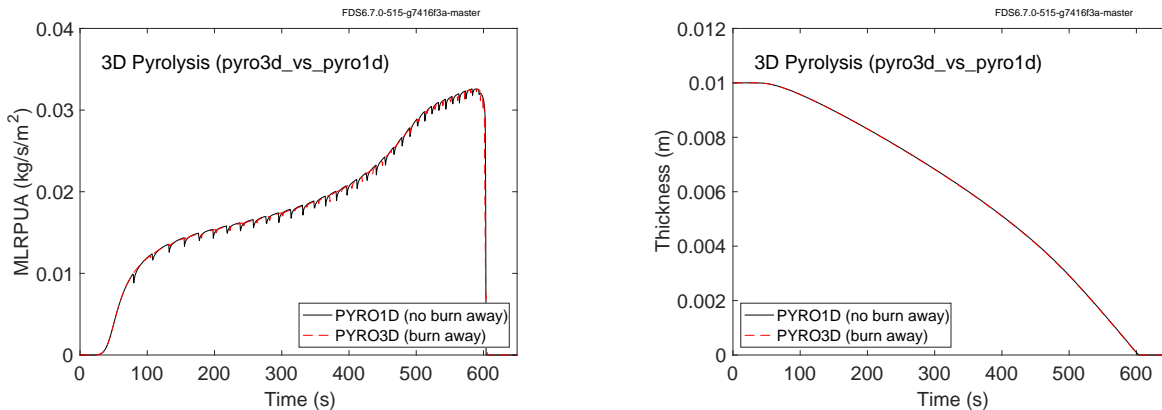

Figure 9: Comparison of thickness in 1D with burn away in 3D. Verification targets are mass loss rate per unit area and material thickness curves.

Mass Transport

This case is a 3D version of the FAA_Polymers_PMMA validation case. A block of black PMMA 0.096 m × 0.096 m × 0.009 m, giving 8.294×10^{-5} m^3, with a bulk density of 1100 kg/m^3, giving 0.0912 kg of total mass, is heated from above with 52 kW/m^2, generating methane as a pyrolysis gas. The diffusion model is used for mass transport. The verification target is to confirm that as the PMMA is consumed the correct amount of methane gets produced. The results are shown below in Fig. 10.
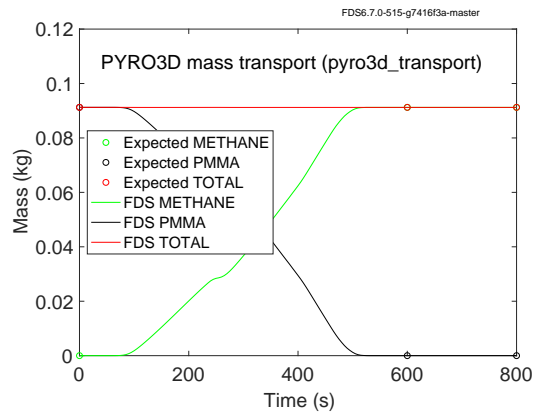
Figure 10: Check of mass conservation in conversion of solid (PMMA) to fuel gas (methane) with burn away using the 3D pyrolysis mass transport algorithm.

CONCLUSIONS

This paper presents ongoing work to develop 3D heat transfer and pyrolysis capabilities in FDS. At present, 3D heat transfer requires full resolution by the grid, which is prohibitive in practice. Therefore, one of our near-term objectives is to implement anisotropic material properties to represent "coarse-grained" transport while retaining the correct thermal inertia of the system. We also plan to couple the 1D and 3D solvers to allow for lateral heat transfer in zero thickness obstructions.

ACKNOWLEDGMENTS

REFERENCES

[1] Andreas Vischer. *Development of a numerical sub-model for the calculation of transient three-dimentional heat transfer in components in fire simulations.* PhD thesis, RWTH Aachen University, 2009. 1

[2] Matthias Siemon. *Ein Pyrolysemodell zur Prognose der Brandausbreitung.* PhD thesis, Technische Universtät Braunwchweig, 2016. 1

[3] S.I. Stoliarov, I.T. Leventon, and R.E. Lyon. Two-dimensional model of burning for pyrolyzable solids. *Fire and Materials*, 38:391–408, 2014. 2

[4] C. Lautenberger. Gpyro3D: A Three Dimensional Generalized Pyrolysis Model. In *Fire Safety Science-Proceedings of the Eleventh International Symposium*, 2014. 2

[5] L. Choe, S. Ramesh, M. Hoehler, M. Bundy, M. Seif, C. Zhang, and J. Gross. National Fire Research Laboratory Commissioning Project: Testing Steel Beams under Localized Fire Exposure. TN 1977, National Institute of Standards and Technology, Gaithersburg, Maryland, 2017. 2

[6] Michael F. Modest. *Radiative Heat Transfer.* Academic Press, second edition, 2003. 3, 5

[7] K. McGrattan, S. Hostikka, R. McDermott, J. Floyd, C. Weinschenk, and K. Overholt. *Fire Dynamics Simulator, Technical Reference Guide, Volume 1: Mathematical Model*. National Institute of Standards and Technology, Gaithersburg, Maryland, USA, and VTT Technical Research Centre of Finland, Espoo, Finland, sixth edition, September 2013. 3, 5

[8] H.S. Carslaw and J.C. Jaegar. *Conduction of Heat in Solids*. Oxford University Press, 2nd edition, 1959. 8, 10

[9] D. Drysdale. *An Introduction to Fire Dynamics*. John Wiley and Sons, New York, 2nd edition, 2002. 8